Water Resources Research

RESEARCH ARTICLE
10.1029/2020WR027918

Angang Li and Jennifer D. Drummond contributed equally to this work.

Key Points:

- Dissolved organic matter (DOM) biological lability decreases with residence time in bioactive regions of the stream (defined as *bioactive residence time*)
- Decreasing biological lability, exchange into and residence times in bioactive regions influence in-stream DOM dynamics
- Model predictions show how the distribution of DOM fractions (i.e., fractionation) and spiraling metrics depend on in-stream location

Supporting Information:

- Supporting Information S1

Correspondence to:

J. D. Drummond,
j.drummond@bham.ac.uk

Citation:

Li, A., Drummond, J. D., Bowen, J. C., Cory, R. M., Kaplan, L. A., & Packman, A. I. (2021). Effect of decreasing biological lability on dissolved organic matter dynamics in streams. *Water Resources Research*, *57*, e2020WR027918. https://doi.org/10.1029/2020WR027918

Received 9 MAY 2020
Accepted 18 DEC 2020

Effect of Decreasing Biological Lability on Dissolved Organic Matter Dynamics in Streams

Angang Li[1], Jennifer D. Drummond[2], Jennifer C. Bowen[3], Rose M. Cory[3], Louis A. Kaplan[4], and Aaron I. Packman[1]

[1]Civil and Environmental Engineering, Northwestern University, Evanston, IL, USA, [2]School of Geography, Earth & Environmental Sciences, University of Birmingham, Birmingham, UK, [3]Earth and Environmental Sciences, University of Michigan Ann Arbor, Ann Arbor, MI, USA, [4]Stroud Water Research Center, Avondale, PA, USA

Abstract Respiration of dissolved organic matter (DOM) in streams contributes to the global CO_2 efflux, yet this efflux has not been linked to specific DOM sources and their respective uptake rates. Further, removal of DOM inferred from longitudinal concentration gradients in river networks has been insufficient to account for observed CO_2 outgassing. We hypothesize that understanding in-stream dynamics of DOM, which is a heterogeneous mixture spanning a wide range of biological labilities, requires considering that DOM lability decreases during downstream transport. To test this hypothesis, we paired seasonal bioreactor measurements of DOM biological lability with whole-stream tracer data from White Clay Creek, Pennsylvania, USA, and used a particle-tracking model to predict in-stream DOM dynamics. The model simulates continuous inputs of DOM and uses storage time in the stream bioactive regions plus kinetic parameters from bioreactors to assess differential uptake of DOM fractions (i.e., fractionation) in the stream. We compared predictions for in-stream dynamics of bulk DOM concentration (quantified as dissolved organic carbon) and fluorescent DOM components. Our model-data synthesis approach demonstrates that more labile fractions of DOM in stream water preferentially originate and are consumed within short travel distances, causing spiraling metrics to change with downstream distance. Our model can account for local sources of rapidly cycled labile DOM, providing a basis for improved interpretation of DOM dynamics in streams that can reconcile apparent discrepancies between respiratory outgassing of CO_2 and longitudinal DOM concentration gradients within river networks.

Plain Language Summary In streams, microorganisms metabolize naturally occurring organic molecules dissolved in streamwater and release carbon dioxide, which contributes to global carbon emissions. These organic molecules are part of a complex and diverse mixture including thousands of different chemical compounds that differ widely in susceptibility to biodegradation. We developed a mathematical model to describe changes in the pool of organic molecules flowing downstream, incorporating field and laboratory measurements of biological degradation of organic molecules and information about water flow into and out of zones that promote biological activity. We demonstrated that the molecules more susceptible to biodegradation are preferentially metabolized and become depleted over short travel distances downstream, while organic species less susceptible to biodegradation are transported farther downstream. Our model improves understanding of the transport and metabolism of organic molecules in streams, and explains factors that control the overall concentration of organic molecules in streams and rivers. The results help to reconcile discrepancies between estimates of carbon dioxide outgassing from streams and observations of organic carbon concentrations within streams.

1. Introduction

Rivers transport substantial amounts of dissolved organic matter (DOM), a large fraction of which is metabolized to CO_2 by microorganisms in streambed biofilms on rocks and sediments (Battin et al., 2016; H. Fischer & Pusch, 2001). At a global scale, rivers are estimated to outgas 1.8 Pg CO_2-C yr^{-1} to the atmosphere (Raymond et al., 2013), which is similar to CO_2 emissions from wetlands and much larger than CO_2 emissions from lakes (Wehrli, 2013). With DOM concentrations in many rivers increasing due to intensive agricultural practices and urbanization (Regnier et al., 2013) as well as the browning phenomenon associated with reductions in acid precipitation (Roulet & Moore, 2006), there is a pressing need to understand microbial uptake of DOM in rivers to understand how CO_2 emissions may change. Microbial uptake of DOM

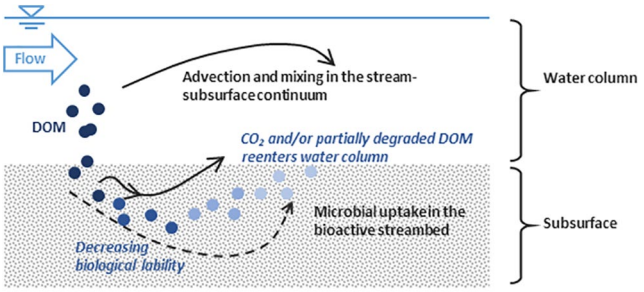

Figure 1. Conceptual model of key processes governing dissolved organic matter (DOM) dynamics in streams. Blue dots represent DOM input at a specific location along the stream, and the color intensity of each dot indicates lability. Advection and mixing vary as a function of the vertical position in the stream-subsurface continuum. The line with a triangle represents the water surface, and the stippled pattern indicates the streambed. Biological lability decreases as a function of the cumulative amount of time that DOM has spent in the bioactive streambed, shown by the shift from dark (high lability) to light (low lability) blue dots. Microbial uptake of DOM leads to either complete degradation to CO_2 or the release of partially degraded DOM back into the water column, where it continues to transport downstream.

depends on DOM lability as well as the exchange of DOM from surface waters into biologically active streambed sediments and other storage areas, which provides the opportunity for microbial uptake during downstream transport (Battin et al., 2008).

DOM processing in streams can be conceptualized as a spiral (Newbold et al., 1982), where DOM derived from terrestrial (allochthonous) or in-stream (autochthonous) sources is transported downstream and into the benthic region where microbial uptake leads to complete degradation to CO_2, and the remainder of the partially or undegraded DOM eventually reenters the water column and continues to transport downstream. An approach used to study DOM spiraling in rivers is to perform whole-stream tracer additions, which have been used to estimate overall DOM uptake. Tracer addition experiments measure the resulting in-stream breakthrough curves (BTCs) at one or more downstream locations, and interpret the BTCs using one-dimensional reach-scale models (Boano et al., 2014; Harvey & Gooseff, 2015). DOM in these studies is measured as a bulk concentration, and therefore the fractions of DOM are not differentiated. Commonly used reach-scale models based on the tracer studies often assume that microbial uptake of DOM occurs at a constant (fixed) rate independent of downstream location (Boano et al., 2014; Newbold et al., 1983; Ward & Packman, 2019). In contrast to this assumption, it is well known that DOM is a heterogeneous mixture spanning a wide range of biological labilities, or in other words varying susceptibility of DOM fractions to be metabolized via microbial uptake and respiration (e.g., Cory & Kaplan, 2012; Sleighter et al., 2014), with increased lability defined as when the same contact time results in increased DOM removal. Furthermore, the lability of the DOM pool decreases as the more labile fractions of DOM are removed and the more recalcitrant fractions remain, demonstrating a need for a model that can account for both spatial and temporal lability variations in streams. However, with the exception of Kaplan et al. (2008), no reach-scale field study has included the range in labilities in the DOM pool when modeling uptake of a DOM tracer (i.e., uptake length) in streams, and lability remained constant in time and space in this model for each of the three defined fractions of DOM.

To bridge this knowledge gap, the objective of this study was to evaluate how lability variations within the DOM pool alter reactivity over time and space and across seasons to influence DOM dynamics in streams. We analyzed these relationships in White Clay Creek, Pennsylvania, USA, where DOM has been extensively studied via *in situ* observations, bioreactor experiments, and in-stream tracer experiments, and lability classes of different DOM fractions have been identified based on relationships between removal rates of dissolved organic carbon (DOC) and fluorescent DOM (FDOM) components with bioreactor residence time (Cory & Kaplan, 2012; Kaplan, 2019; Kaplan & Newbold, 1995; Kaplan et al., 2008). We used FDOM, associated with microbially- and terrestrially-derived humic DOM and protein-like FDOM linked to free or combined amino acids (Cory & Mcknight, 2005), as proxies for the range of labilities within the DOM pool. Conventionally, protein-like FDOM is a proxy for the most labile DOM, while humic-like FDOM is a proxy for less labile DOM (Balcarczyk et al., 2009; Fellman, Hood, Edwards, et al., 2009; Hood et al., 2009). We linked these bioreactor lability measurements to in-stream dynamics using a particle tracking model approach that supports consideration of temporal and spatial variations in reaction rate and flow parameters at the reach scale (Li et al., 2017).

The key processes considered to govern DOM dynamics in White Clay Creek are visualized in a conceptual model: advection and mixing bring DOM into the bioactive part of the stream-subsurface continuum, resulting in microbial uptake and modification of DOM (Figure 1). With application to White Clay Creek, we focus only on microbial reaction in the bioactive streambed as benthic respiration in headwater streams exceeds water column respiration by over two orders of magnitude (Minshall et al., 1983) with photochemical alteration rates much lower than biodegradation rates of labile DOC in this stream (Bowen et al., 2020). We constructed the quantitative model to study the combined impacts of lability variations within the DOM

pool, exchange into and residence times in bioactive regions that together influence DOM dynamics in streams. DOC and FDOM decreasing labilities with bioactive residence time were quantified for different months of the year, to span the wide temporal differences in DOM lability in rivers (Fellman, Hood, D'amore, Edwards, et al., 2009; Harun et al., 2016; Masese et al., 2017; Singh et al., 2014). The model-data synthesis approach was first applied to a ^{13}C-DOC tracer study, with data available in both the bioreactor lab-scale and stream reach-scale. The same approach was then used to predict seasonal differences in DOM dynamics and spiraling metrics, such as uptake length and velocity, and the distribution of DOM fractions (i.e., fractionation) during downstream transport. Finally, we used the model to assess the relative contribution of upstream sources to reflect the local stream water DOM signature observed at a site downstream.

2. Methods

We evaluated the combined effects of in-stream DOM transport, exchange into and residence times within the bioactive region, and decreasing biological lability with residence time on DOM dynamics in White Clay Creek (Section 2.1). For each season, decreasing biological lability was estimated from measurements of DOC concentration and intensity of FDOM components in laboratory bioreactor experiments (Section 2.2). These results were paired with a field tracer injection study that characterized the hydrologic conditions during each experiment (Section 2.3). A particle tracking model (Section 2.4) was used to characterize in-stream transport, exchange into and residence time in the bioactive region based on the observed tracer dynamics (Section 2.5.1). The model was then used to project reach-scale ^{13}C-DOC in-stream BTCs (Section 2.5.2) using the combined lab-based ^{13}C-DOC lability rate parameters and reach-scale hydrologic parameters. This model-data synthesis approach was then used to predict seasonal variations of DOM dynamics in White Clay Creek for both point-sources and distributed sources of DOM (Section 2.6).

2.1. Field Site Description

White Clay Creek is a third-order stream in the southeastern Pennsylvania Piedmont that drains agricultural lands, and despite an intact riparian forest, the stream water is enriched in nutrients (Newbold et al., 1997). Mean seasonal DOC concentration ranges from 1.3 mg C L^{-1} in winter to 1.7 mg C L^{-1} in summer at baseflow conditions (Hullar et al., 2006). Monthly average stream water temperature ranges from 3.1°C in January to 18.6°C in July. White Clay Creek has mean annual stream discharge ranging from 66 to 156 L s^{-1} (Newbold et al., 1997). Streambed sediments are predominantly gravel-cobble, with sand and finer sediments also present in large quantities. Hydraulic conductivity ranges from 1.8×10^{-5} m s^{-1} to 1.1×10^{-4} m s^{-1} (Battin et al., 2003), and streambed porosity ranges from 20% to 30% (Battin et al., 2003; Sawyer et al., 2014).

2.2. Bioreactor Laboratory Experiments

2.2.1. ^{13}C-DOC Tracer Experiment

We compiled published data from a bioreactor experiment conducted on October 4, 2002, which measured the concentrations of biodegradable DOC in stream water and uptake of natural stream water amended with a ^{13}C-DOC tracer as a function of empty-bed contact time or residence time in the bioreactors filled with sintered glass beads, calculated as the volume of the bioreactor divided by the flow rate of water pumped through the bioreactor (Kaplan et al., 2008, 2019). The ^{13}C-DOC tracer was prepared from tulip poplar tree tissues (*Liriodendron tulipifera)* and was highly labile (i.e., more susceptible to microbial metabolism) compared to the natural DOM pool in the stream water. The source of microbes and carbon do not differ between the streambed and the bioreactors. The bioreactor laboratory experiments are described in more detail in the supporting information (Text S1).

2.2.2. Natural Streamwater Experiments

To characterize uptake of DOC and FDOM components from natural stream water, we conducted additional bioreactor experiments on August 4, 2016, November 3, 2016, January 26, 2017, and May 23, 2017 following the same approach used by Kaplan et al. (2008), Cory and Kaplan (2012), and Sleighter et al. (2014) (Text S1). The use of FDOM to study DOM dynamics in streams is supported by correlations between optical

properties and molecular properties of DOM in White Clay Creek (Sleighter et al., 2014). Briefly, influent and effluent FDOM was characterized using excitation emission matrix spectroscopy that measures fluorescence intensities as Raman units (RU) over a range of excitation and emission wavelengths. Excitation emission matrices were evaluated using a multivariate technique, parallel factor analysis, that decomposes the matrices into five chemically independent fluorescent components, C1–C5. The five FDOM components, previously validated for White Clay Creek (Cory & Kaplan, 2012, Text S1, Figure S1, Table S1), are commonly identified in freshwaters (Cory & Mcknight, 2005; Osburn et al., 2012; Parr et al., 2014, 2015; Stedmon & Markager, 2005). C1–C3 are humic-like FDOM components, with C1 associated with recent microbially derived DOM, and C2 and C3 associated with terrestrially derived DOM; C4 resembles tryptophan and C5 resembles tyrosine, both being protein-like FDOM components (Cory & Kaplan, 2012, Figure S1, Table S1).

2.2.3. Calculations of Biological Lability

Biological lability is the susceptibility of DOM to be metabolized by microbial communities. To quantify decreasing lability with residence time from bioreactor measurements, for each separate experiment we fit the measured ^{13}C-DOC (Section 2.2.1, Figure S2), DOC concentration (C) or FDOM intensity of each component (Section 2.2.2, Figure S3) versus residence time in bioreactor (τ) using a reactivity continuum model $\frac{C_\tau}{C_0} = \left(\frac{\alpha}{\alpha+\tau}\right)^{\nu}$ for ^{13}C-DOC, DOC or each FDOM component, where α and ν are fitting parameters that describe the reaction rates (Boudreau & Ruddick, 1991; Koehler et al., 2012). The apparent rates (sensu Boudreau & Ruddick, 1991) apply to the bulk DOM concentration and represent the weighted average of actual reaction rates for all DOM in the system. As such, the apparent rate is not first-order, but rather an ensemble average of first-order reaction rates that change with time. The reactivity continuum model assumes a continuum of labilities with validity beyond timescales of measurements, and is thus able to predict the decrease in apparent reaction rates over time in a realistic and robust manner (Koehler et al., 2012; Vähätalo et al., 2010). We calculated the apparent first-order reaction rate constant $k_{T0} = \frac{\nu}{\alpha+\tau}$ (Boudreau et al., 2008) at a reference water temperature (T_0 = 20°C, 293.15 K), as a function of residence time in the bioreactors. The fitted values of α and ν for ^{13}C-DOC in October 2002 and seasonal experiments in August 2016, November 2016, January 2017, and May 2017 for DOC concentration (C) and each FDOM component are reported in Table S2.

Bioreactor experiments were performed at a constant temperature and thus did not account for seasonal variations in stream water temperature, which is important for seasonal changes in microbial reaction rates (Caissie, 2006; Phinney & Mcintire, 1965). To correct for seasonal changes in stream water temperature, we applied a universal temperature-dependence of metabolism (Gillooly et al., 2001), $k = k_{T0}e^{\frac{E(T-T_0)}{k_BTT_0}}$, where k is the temperature-adjusted apparent first-order reaction rate constant, T is water temperature in Kelvin, T_0 is a reference water temperature (20°C, 293.15 K), k_B is Boltzmann's constant (8.617×10^{-5} eV K^{-1}), and E is activation energy that has been consistently reported to be ~0.6 eV for a wide range of thermal histories and microbial communities (Brown et al., 2004; Demars et al., 2011; Perkins et al., 2012, but see; Wetler et al., 2015). Stream water temperature was not measured on October 4, 2002, so we used the historical average stream water temperature for the month October (11.7°C).

The relationships between k and residence time in the bioreactors were used to parameterize reaction (i.e., decreasing biological lability with residence time) in the particle tracking model for in-stream DOM dynamics (Section 2.4) (Figure 1). Figure S2b shows k as a function of residence time in bioreactor for the ^{13}C-DOC experiment. Figures S3b and S4b show k as a function of residence time in the bioreactor for natural stream water (DOC concentration and each FDOM component) for the August 2016, November 2016, January 2017, and May 2017 experiments. For the purpose of modeling, we assumed that the reaction rate constants for DOM once in the bioactive region of the streambed were identical to the reaction rate constants of DOM calculated from the bioreactors. While these are the best available estimates of the lability kinetics of DOM fractions in White Clay Creek, there are expected differences between the bioreactors and streambed sediments (described in detail in supplemental Text S1). Continuous perfusion with stream water and suspended microorganisms facilitated colonization of the sintered bead matrix in the bioreactors, resulting in

gradients of microbial densities, activities, and species composition analogous to the bioactive porous environment in the streambed (Kaplan & Newbold, 1995). The residence time in a bioreactor is analogous to the cumulative residence time of DOM in the bioactive region of the streambed. The bioreactors reflect an undisturbed environment with at least twice the density of bacterial cells found in the streambed (Kaplan and Bott, 1989; Wiegner et al., 2015). Even though differences between the model output and reach-scale field data results were expected due to the different local environmental conditions within the bioreactor and streambed sediments, we are still able to demonstrate key process controls on DOM dynamics in streams with consideration of a continuum of DOM lability pools into a reach-scale model.

2.3. Field Tracer Injection Experiments

2.3.1. ^{13}C-DOC Experiment

Paired with the ^{13}C-DOC bioreactor experiment, field experiments of conservative solute (Br^-) and ^{13}C-DOC tracer injections to characterize hydrologic conditions and estimate reach-scale DOC uptake were simultaneously conducted on October 2, 2002, in White Clay Creek at ~1,264 m upstream of the bioreactor water sampling site under baseflow conditions (Kaplan et al., 2008, 2019). In-stream Br^- BTCs and discharge were measured at x = 15, 51, 426, and 1,265 m downstream of injection, and the in-stream concentrations of ^{13}C-DOC were measured during the peaks of the Br^- BTCs at x = 15, 30, 87, 147, 250, 426, 724, and 1,265 m downstream of injection, where $x = 0$ is the injection location. The background corrected BTCs are reported in the supporting information (Figure S5). The discharge was 12.8 L s^{-1} at 15 and 51 m, 14.3 L s^{-1} at 426 m, and 17.6 L s^{-1} at 1,265 m downstream of injection.

2.3.2. Solute Tracer Experiments to Estimate Hydrologic Conditions

Solute tracer (NaCl) experiments were conducted under similar hydrologic conditions as each date of the natural stream water sample collection and bioreactor experiments. The field experiments of NaCl (detectable at 2 μS/cm, equivalent to 1 mg L^{-1} NaCl) were conducted on July 23, 2014 in different reaches of White Clay Creek, following the same method in Battin et al. (2003). NaCl was injected at ~602 m downstream and ~812 m upstream of the bioreactor water sampling site, where baseflow discharge was 82 and 62 L s^{-1} respectively. Background concentrations, measured immediately prior to the injections, were subtracted from the tracer BTCs. Although the dates of solute tracer and bioreactor experiments were different, we paired seasonal bioreactor measurements with solute tracer data by matching the stream discharge (Table S3). January and May had similar hydrologic conditions and were paired with the same tracer data (Q = 82 L s^{-1}), while August and November had similar hydrologic conditions and were paired with the same tracer data (Q = 62 L s^{-1}) (Table S3). Concurrent with each tracer experiment, reach characteristics were estimated for each study reach, following the method of Battin et al. (2003): stream cross-sectional area was estimated from conservative BTCs using the One-Dimensional Transport with Inflow and Storage (OTIS) model (Runkel, 1998); stream width was averaged from measurements at 10–20 transects; stream depth was estimated from cross-sectional area and stream width; river slope was measured along the thalweg; median sediment grain size (D_{50}) was visually estimated. Reach characteristics identified from the tracer experiments are summarized in Table S4. In addition, we estimated best fits of the conservative BTCs from July 2014 experiments using the OTIS model (Runkel, 1998), which served as a baseline to estimate stream hydrologic parameters (Section 2.5.1).

2.4. Particle Tracking Model

Reach-scale dynamics were simulated using a numerical particle tracking model that is able to represent decreasing DOM labilities dependent on residence times at the reach scale, and generate extensive spatial and temporal information that cannot be obtained from whole-stream injections or reach-averaged models (Li et al., 2017). The particle tracking approach discretizes solute mass into "virtual particles," which are subject to preassigned velocity distributions, hydrodynamic mixing rates, and reaction rates. The particle tracking model is defined in two dimensions: the downstream direction and the vertical direction spanning the stream-subsurface continuum. A complete description of the model framework is presented in Text S2. Matlab R2018a (Version 9.4) was used for all modeling and analysis.

2.5. Model Application to White Clay Creek

2.5.1. Parameterization of Hydrologic Conditions

To characterize the nonreactive in-stream transport and mixing in the subsurface, the solute tracer experiments from October 2002 (Section 2.3.1) and July 2014 (Section 2.3.2) were fit using the particle tracking model. Briefly, for each data set, we used the measured reach characteristics (Table S4) to parameterize the transport part of the particle tracking model, that is velocity and mixing only. We then used the measured conservative BTC to fit the model's transport parameters that were not directly measured in the field. These fits provide best-available-estimates of stream transport conditions during each tracer study. To simulate a continuous injection experiment, we injected 10,000 numerical particles, uniformly distributed in the water column at $x = 0$, at each time step during the continuous injection. Details on the fitting procedure are included in the supporting information (Text S2), with best fits shown in Table S5 and Figures S5 and S6.

2.5.2. Model Projections Combining Decreasing Biological Lability and Hydrologic Conditions as Input Parameters

We applied a model-data synthesis approach to analyze DOM dynamics in White Clay Creek for October 2002 by combining parameters estimated from bioreactor data and field tracer data in the particle-tracking model. Specifically, the hydrologic conditions were parameterized from the field tracer data, and the residence-time-dependent reaction rates, representing decreasing biological lability, were parameterized from the bioreactor data. To first assess the model conceptualization, without any fitting of the ^{13}C-DOC BTCs, the simulated in-stream ^{13}C-DOC concentration is consistent with the observed concentration within a factor of 3 (0.6–2.8) at all sampling locations (Figure S4). In particular, the model is able to match observed ^{13}C-DOC concentration reasonably well at locations beyond $x = 426$ m, while underestimating observed DOC concentration at locations closer to the injection point. The underestimation of observed DOC concentrations is a direct result of an overestimation of in stream reaction rate constants derived from the ^{13}C-DOC bioreactor data (Section 2.2). The overestimated uptake is most pronounced at locations relatively close to the injection point, which have relatively short bioactive residence time and relatively high ^{13}C-DOC lability. Nevertheless, the overall correspondence between the model output and observations for both Br^- and ^{13}C-DOC of the October 2002 data set indicates that the model is able to represent key controls on the transport and uptake of DOM in White Clay Creek that demonstrate how decreasing biological lability incorporated into a reach-scale model influences DOM dynamics in streams. We therefore use this model conceptualization to assess seasonal patterns of DOM uptake in White Clay Creek, to gain understanding on how decreasing lability influences DOM fractionation at the reach-scale, which cannot yet be measured directly.

2.6. Model Predictions of Seasonal DOM Dynamics

2.6.1. Point Source Input

Following the same approach described above (Section 2.5.2), we used the particle tracking model to assess seasonal dynamics of DOC and each FDOM component using data from August 2016, November 2016, January 2017, and May 2017. For each season, we simulated a continuous tracer injection to a 10 km reach using the particle tracking model with best-fit transport parameters for conservative BTCs (Section 2.5.1, Table S5), reaction rate constants based on bioreactor data (Section 2.2.3, Table S2), and DOC concentration and the FDOM intensity measured in White Clay Creek. We simulated in-stream BTCs of conservative solute, DOC, and FDOM every 10 m along the 10 km reach, as well as the steady state concentrations (i.e., plateau concentrations in BTCs). We also recorded the distribution of bioactive residence time as well as the total residence time in the stream at 0, 100, 500, and 1,000 m downstream of the injection source.

We normalized the simulated input DOC concentrations and FDOM intensities to those measured in White Clay Creek at the site and date of the injection. From the simulated concentration or intensity gradients of DOC and FDOM, respectively, we calculated the following parameters:

- uptake length $S_w = \frac{1}{k_w}$, where $k_w = -\left(1 / C\right)\partial C / \partial x$, x is downstream distance, and C is DOC concentration (or intensity of FDOM in Raman Units [RU])
- uptake velocity $v_f = \frac{Q}{WS_w}$, where Q is discharge and W is river width, and

- areal uptake rate $U = v_f C$

Uptake length, which is sensitive to stream flow, represents the average downstream distance traveled before microbial uptake (Newbold et al., 1981). Uptake velocity is the apparent mass transfer coefficient (Stream Solute Workshop, 1990) representing the rate (as a vertical "piston velocity" at which DOC or FDOM is removed from the water column to the bioactive streambed). Conventionally, k_w is estimated as the exponential rate of longitudinal decline in the concentration of an injected tracer, but this approach applies to a single substance, for example, ^{13}C-glucose or ^{13}C-acetate, with a single characteristic uptake rate and does not apply to a concentration consisting of a mixture of substances of varying labilities or whose lability varies with time (Newbold, 1992). Given that DOM is a mixture of molecules with various labilities, the simulated uptake rate diminishes with downstream distance with the more rapid loss of the more labile forms. We therefore estimated k_w from the local slope at any given distance. The local slope refers to ln (C/C_{solute}) as a function of x, at any given distance, where C_{solute} is the conservative solute tracer concentration. This is in contrast to the conventional method that estimates k_w as the exponential rate constant of the longitudinal decline in concentration, that is, a constant slope of ln (C/C_{solute}) as a function of x over the entire reach. This approach becomes identical to the conventional one when the assumption of exponential decline in concentration is met.

The values of the spiraling metrics calculated for the point of injection are those applicable to the bulk DOC as sampled from the stream and therefore represent the model estimates of reach-scale S_w, v_f, and U for the stream. Metrics calculated for successive downstream distances from the injections represent properties of the fraction of the injected DOC that remain in the water column after traveling the respective distance. They do not describe a property of the stream at that point because the DOC simulated to have been removed has likely been replaced via lateral and in-stream sources. The simulated injection point (and location from which the bioreactor samples were drawn) lies near the lower end of a 2-km reach in which bulk DOC concentration is longitudinally uniform (e.g., increasing over the reach by 0.05 mg/L or 3.3% on October 2, 2002; Kaplan et al., 2008). We therefore infer that DOC uptake was approximately in balance with lateral and in-stream sources, and that both uptake and sources were uniformly distributed throughout the reach. In addition to spiraling metrics, we calculated the removal of DOC and each FDOM component by taking the difference of simulated in-stream concentrations between the conservative tracer and DOC or FDOM at each downstream location. Further, we compared the fraction of time spent in the bioactive region (i.e., the ratio of bioactive residence time to total residence time) in different seasons at $x = 100$, 500, and 1,000 m downstream using the nonparametric Wilcoxon rank-sum test. At each downstream location, the reach-averaged k was estimated using the relationships derived from the bioreactor experiments for total DOC and total FDOM (Figure S4a).

2.6.2. Distributed DOC Inputs

To simulate distributed DOM inputs that often occur in natural streams, we added point source continuous injections distributed each 10 m along the 10 km reach. Although the exact locations of DOM sources to White Clay Creek are unknown, this analysis evaluates the combined influence of transport and mixing in the subsurface, residence times in the bioactive region, and decreasing biological lability with residence time that control DOM distributions. We used this model to assess how far upstream each DOM fraction could potentially be sourced. To quantify the relative contribution of each upstream source, we recorded the fraction of FDOM intensity sampled at $x = 10$ km that originated from each upstream source location. This distribution is the discrete probability density function of upstream source locations. We then estimated the continuous probability distribution of upstream inputs by fitting a continuous distribution through the discrete probability density function of upstream source locations. We used this method to calculate the upstream distribution of contributing sources for each FDOM component.

3. Results

We use a model-data synthesis approach that combines hydrologic reach-scale parameters with biological lability rate parameters estimated from bioreactor experiments to predict seasonal variations of DOM dynamics in streams. The simulations show the combined influence of hydrologic transport, residence time in bioactive regions, and decreasing biological lability, which is not yet possible to measure directly in streams.

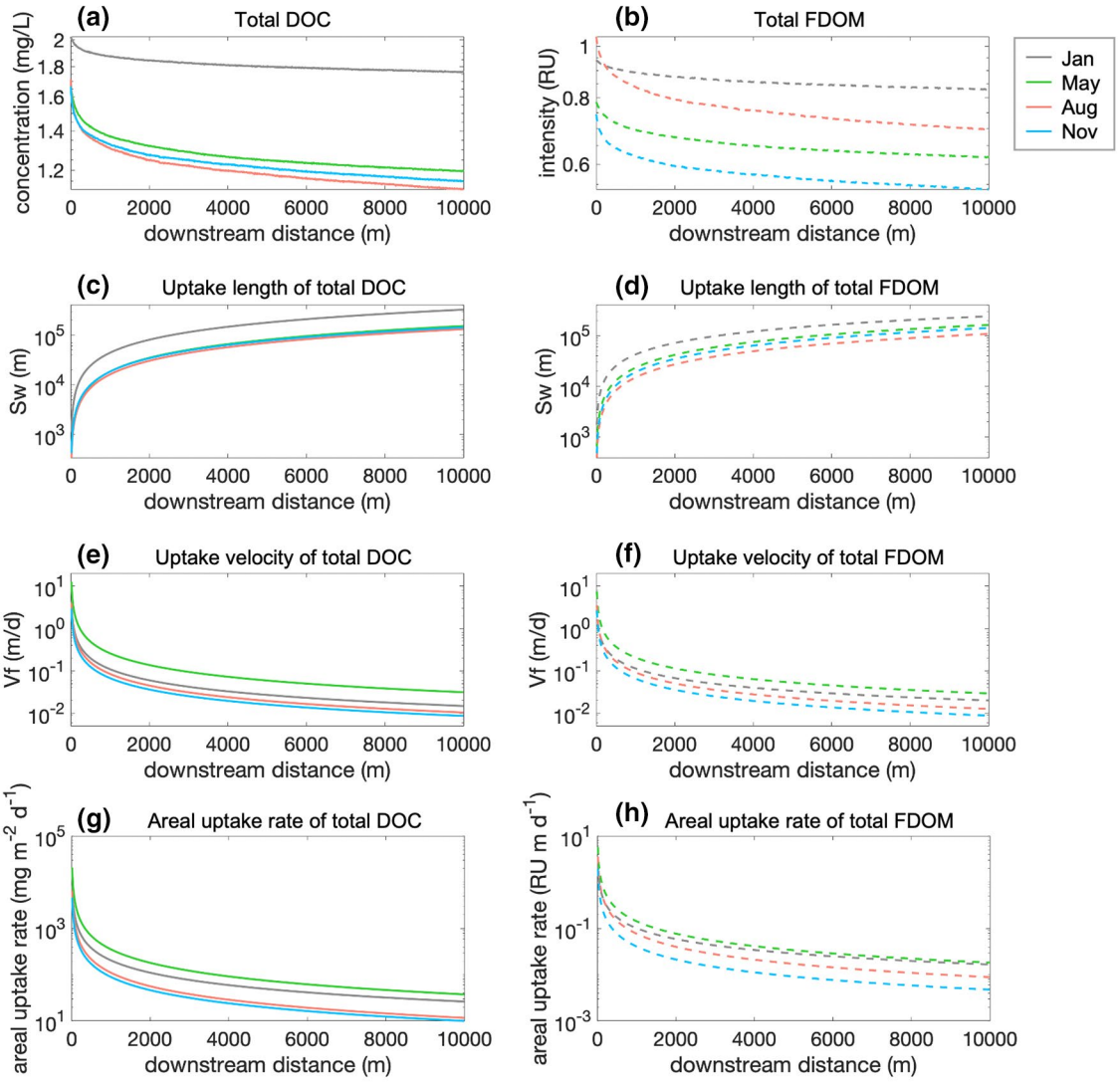

Figure 2. In-stream concentration and intensity of the injected dissolved organic carbon (DOC) and total fluorescent dissolved organic matter (FDOM) that passed $x = 0$ (a and b), uptake length (c and d), uptake velocity (e and f), and areal uptake rate (g and h) as a function of downstream distance of a point source continuous injection at steady state, simulated under transport and reaction conditions in August 2016, November 2016, January 2017, and May 2017. Left panels represent DOC concentration, and right panels represent total FDOM intensity (i.e., sum of C1–C5 in Raman Units [RU]). Vertical axes are in $\log_{10}$ scale to improve visualization of the wide range in observed values.

We first assess the seasonal variations of DOC and total FDOM uptake (Section 3.1) and then evaluate FDOM fractionation (Section 3.2), describing in detail the uptake of each FDOM component C1–C5. We then assess how DOM distributed sources and variations in biological lability of different FDOM components upstream determine the DOM signal observed at a downstream location (Section 3.3).

3.1. Seasonal Variations of DOM Uptake from a Continuous Point Source

In all seasons (January, May, August, and November), the simulated concentration of DOC and total FDOM decreased with downstream distance, and the decrease was faster (i.e., a steeper gradient) at locations closer to the injection source (Figures 2a and 2b). A faster decrease in DOC concentration and total FDOM intensity (i.e., sum of C1–C5 in Raman Units [RU]) occurs because of faster hydrologic transport into and longer retention in bioactive regions and/or increased uptake within these regions that is linked in the

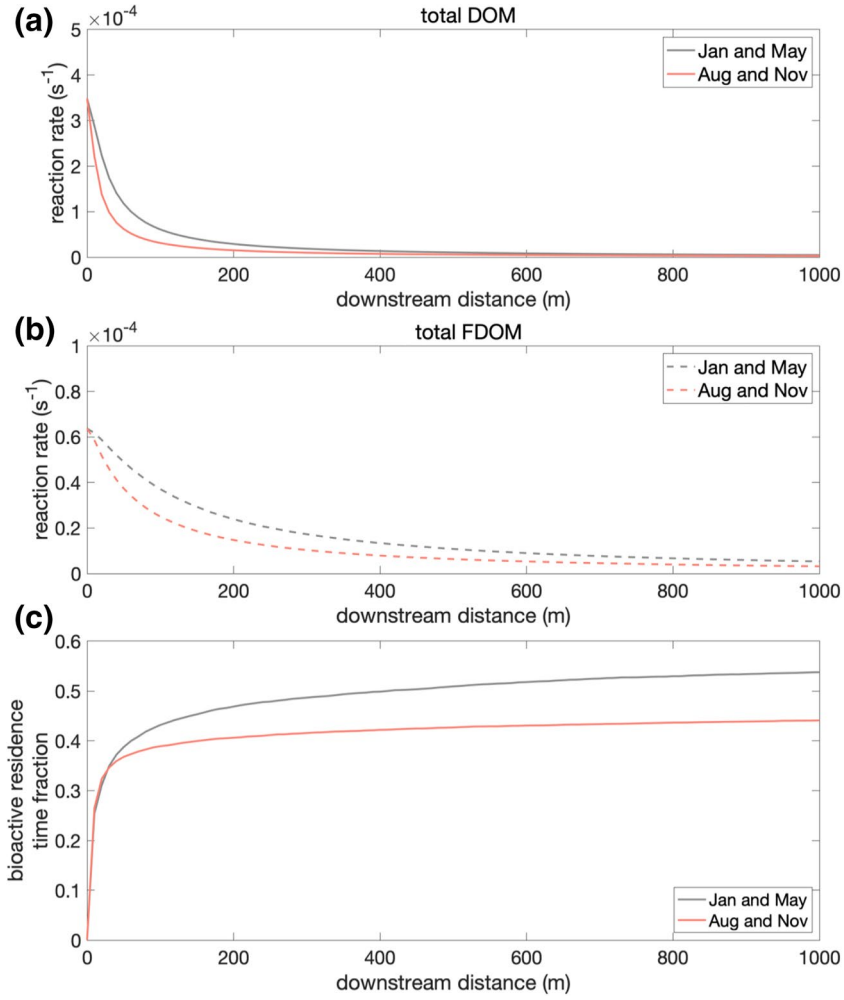

Figure 3. Reach-averaged k for (a) total dissolved organic matter (DOM), (b) total fluorescent dissolved organic matter (FDOM), and (c) fraction of time transported DOM spent in the bioactive region (i.e., bioactive residence time fraction) versus downstream distance of a point source continuous injection at steady state, grouped by hydrologic conditions (August/November and January/May).

model to biological lability, which we can differentiate between when comparing seasons. January had the lowest gradient of DOC and total FDOM decline over downstream distance, with 13% reduction of in-stream DOC concentration and 12% reduction of in-stream total FDOM intensity between the injection and 10 km downstream. In August, DOC concentration and total FDOM intensity were relatively high near the injection source, but decreased rapidly over downstream distance, with 34% reduction of tracer DOC concentration and 33% reduction of total FDOM intensity between the point source and 10 km downstream. Consequently, uptake length increased with downstream distance, with the most rapid increase occurring close to the source (Figures 2c and 2d). In January, the uptake length (S_w) of DOC increased from 1 km at $x = 0$ m to 325 km for the DOC remaining in the water column at $x = 10$ km. In August, DOC uptake length increased from 0.3 km at $x = 0$ m to 131 km at $x = 10$ km (Table 1). Similar to the trend in uptake length, uptake velocity (v_f, Figures 2e and 2f) and areal uptake rate (U, Figures 2g and 2h) decreased with downstream distance in all seasons. On average, uptake velocity decreased by 97% within the first kilometer. Total FDOM had similar uptake lengths and uptake velocities as DOC.

The fraction of time that transported FDOM spent in the bioactive region (which we define as the bioactive residence time fraction) increased with downstream distance while the reach averaged k decreased with distance from the source (Figure 3). When grouped by hydrologic conditions (i.e., January/May and August/November), the bioactive residence time fractions in January/May were significantly higher than those in

Table 1
Spiraling Metrics Calculated at x = 100 m, 1 km, 5 km, and 10 km Under Transport and Reaction Conditions in August 2016, November 2016, January 2017, and May 2017

(A) Uptake length (S_w)

	S_w of DOC (km)					S_w of FDOM (km)				
	0 m	100 m	1 km	5 km	10 km	0 m	100 m	1 km	5 km	10 km
January	1	6	44	179	325	2	8	43	143	241
May	0.4	2	19	81	152	0.6	3	23	90	162
August	0.3	2	16	70	131	0.4	2	15	60	108
November	0.4	2	19	77	143	0.5	3	19	77	141

(B) Uptake velocity (v_f)

	v_f of DOC (m d^{-1})					v_f of FDOM (m d^{-1})				
	0 m	100 m	1 km	5 km	10 km	0 m	100 m	1 km	5 km	10 km
January	4.3	0.77	0.11	0.03	0.01	2.8	0.62	0.11	0.03	0.02
May	12.6	2.0	0.26	0.06	0.03	7.4	1.39	0.21	0.05	0.03
August	4.0	0.66	0.08	0.02	0.01	3.5	0.64	0.09	0.02	0.01
November	2.9	0.50	0.07	0.02	0.01	2.7	0.47	0.07	0.02	0.01

(C) Areal uptake rate (U)

	U of DOC (g m^{-2} d^{-1})					U of FDOM (10^{-6} RU m d^{-1})				
	0 m	100 m	1 km	5 km	10 km	0 m	100 m	1 km	5 km	10 km
January	8.6	1.5	0.20	0.05	0.03	2.61	0.58	0.10	0.03	0.02
May	20.7	3.2	0.35	0.07	0.04	5.77	1.05	0.14	0.03	0.02
August	6.6	0.98	0.11	0.02	0.01	3.61	0.61	0.08	0.02	0.01
November	4.7	0.75	0.09	0.02	0.01	1.94	0.32	0.04	0.01	0.005

Abbreviations: DOC, dissolved organic carbon; FDOM, fluorescent dissolved organic matter.

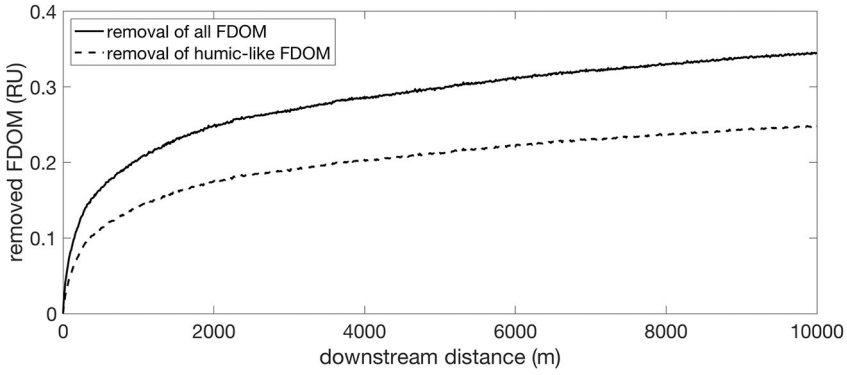

Figure 4. Removal of total fluorescent dissolved organic matter (FDOM) (i.e., sum of the C1–C5 intensity difference in Raman Units (RU) between $x = 0$ and a distance downstream) compared to the removal of humic-like FDOM (i.e., sum of the C1–C3 intensity difference in Raman Units (RU) between $x = 0$ and a distance downstream) as a function of downstream distance of a point source continuous injection at steady state, simulated under transport and reaction conditions in August 2016. Humic-like FDOM was responsible for most of the total FDOM removed.

Table 2
Total DOC, Total FDOM, and FDOM Components Removed Prior to Reaching 10 km Downstream of a Point Source Continuous Input, Simulated Under Transport and Reaction Conditions in August 2016, November 2016, January 2017, and May 2017

(A) Intensity or concentration removed

	January	May	August	November
DOC (mg/L)	0.26	0.47	0.60	0.52
FDOM (RU)	0.12	0.17	0.34	0.21
C1 (RU)	0.06	0.08	0.18	0.09
C2 (RU)	0.01	0.02	0.03	0.01
C3 (RU)	0.01	0.02	0.04	0.03
C4 (RU)	0.02	0.02	0.05	0.03
C5 (RU)	0.02	0.03	0.04	0.05

(B) Percentage removed

	January	May	August	November
DOC	13%	28%	35%	31%
FDOM	12%	21%	33%	28%
C1	11%	20%	32%	25%
C2	10%	18%	29%	20%
C3	10%	20%	29%	26%
C4	10%	15%	29%	22%
C5	29%	48%	66%	58%

Abbreviations: DOC, dissolved organic carbon; FDOM, fluorescent dissolved organic matter.
Notes. Results shown between $x = 0$ and 10 km as a (A) difference in intensity or concentration and (B) percentage. C1–C3 represent humic-like FDOM; C4 and C5 represent protein-like FDOM (Table S1, Figure S1).

August/November at all downstream locations (Wilcoxon rank-sum test, $p < 0.001$). In January and May, the bioactive residence time fraction averaged ($\pm 1\sigma$) 0.43 ± 0.19, 0.51 ± 0.15, and 0.54 ± 0.13 at $x = 100$ m, $x = 500$ m, and $x = 1{,}000$ m respectively, compared to 0.39 ± 0.13, 0.43 ± 0.11, and 0.44 ± 0.10 in August and November. These results indicate that there was generally more hydrodynamic mixing and increased residence time in the bioactive streambed in January and May versus August and November. However, uptake velocity (v_f) and areal uptake rate (U) parameters, which reflect the combined influence of lability and hydrologic conditions, were consistently higher in January/May compared to August/November at all downstream locations for both DOC and total FDOM (Figures 2e–2h; Table 1). Increased uptake velocity and areal uptake rates correspond with a shorter travel distance before DOM is taken up. This result is due to the higher bioactive residence time fraction in January/May compared to August/November since reaction rate constants were generally lower in January/May than in August/November (Figure 3, Figure S3b).

3.2. Reach-Scale Fractionation of FDOM Components from a Continuous Point Source

FDOM was removed throughout the reach, as estimated by the difference in intensity in Raman Units (RU) from $x = 0$ and a known distance downstream. Figure 4 shows the removal of total FDOM (i.e., sum of the removal of C1–C5) compared to the removal of humic-like FDOM (i.e., sum of the removal of C1–C3) over distance downstream of a continuous point source, under August transport and reaction conditions. The removal of total FDOM increased from 0.2 RU at 1 km to 0.34 RU at 10 km, while the removal of humic-like FDOM increased from 0.14 RU at 1 km to 0.25 RU at 10 km. Therefore, humic-like FDOM was responsible for most of the total FDOM removed, which was observed for all seasons (Table 2A). Specifically, humic-like FDOM contributed to 67% of total FDOM removed in January, 71% in May, 74% in August, and 62% in November (Table 2A). However, if we instead assess the percentage removed of each FDOM component from $x = 0$–10 km downstream, removal of C1, C2, C3 (humic-like FDOM) was 10%–11% in January and 29%–32%

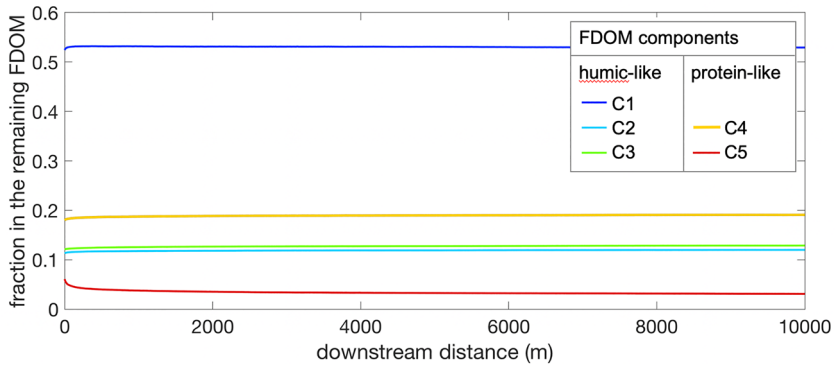

Figure 5. Remaining fraction of each fluorescent dissolved organic matter (FDOM) component as a function of downstream distance from a point source continuous injection at steady state, simulated under transport and reaction conditions in August 2016.

in August, while C4 and C5 (protein-like FDOM) removal was 10%–29% in January and 29%–66% in August (Table 2B). Therefore, despite humic-like FDOM being known as a proxy for less labile DOM, and a lower percentage removed from 0 to 10 km downstream, its high abundance (60%–75% of total in-stream FDOM, Figure S3a) led to humic-like FDOM accounting for most of the total FDOM removed for all seasons.

When we instead observe the remaining fraction of each FDOM component (i.e., in-stream ratio of intensity of each component to total FDOM that was not removed), the fractions are similar at all locations downstream except for very near to the source (Figure 5) and for all seasons (Table 3). The initially steeper portion of each curve in the first ~100–200 m downstream of the source (Figure 5) reflects the preferential uptake of the most labile fractions. These results demonstrate how decreasing biological lability with residence time alters the in-stream DOM signature close to the source, but that further from the source can be more controlled by variations in hydrologic conditions, as seen by seasonal variations in bioactive residence times and total percent removed (Figure 3, Table 2B). For instance, the in-stream fraction of tyrosine-like FDOM (C5) decreased by 18% from 0.061 at the injection (0 km) to 0.031 at 10 km. In comparison to C5, the fraction of tryptophan-like FDOM (C4) increased by 7% from 0 to 10 km. Tryptophan-like FDOM contributed consistently 18%–19% to in-stream FDOM 10 km downstream of the injection, and overall contributed to a greater fraction of the remaining FDOM than either humic-like FDOM components C2 or C3, although still less than C1.

3.3. Reach-Scale Fractionation of FDOM Components from Distributed Continuous Inputs

Since fractionation was similar at 10 km for all seasons (Table 3), we present only May as an example to demonstrate model predictions of the relative contribution of upstream sources of each FDOM component to the stream water DOM signature observed at a site downstream. Figure 6 shows the probability density function of upstream contributing sources within the 10 km reach (shown on the y-axis as from 0 to −10 km upstream) for each FDOM component in May. A conservative tracer has the same probability of originating from each upstream distance, because the inputs are uniform throughout the reach (i.e., the black line in Figure 6 does not change with distance upstream of the source). In contrast to a conservative tracer, C5 had the highest lability (Figure S2). Accordingly, the probability of C5 originating from each upstream source differed from a conservative tracer. The probability of C5 originating from sources close to the observation location ($x = 0$) was high (i.e., the red line in Figure 6 is highest near $x = 0$ and decreases with distance upstream from 0 to −10 km), because C5 originating from farther upstream was preferentially removed in the stream. C4 lability decreased rapidly over time, and quickly became one of the least labile components (Figure S2). As a result, C4 sources were almost uniformly distributed within the 10 km reach (i.e., yellow line in Figure 6 shows less variation from 0 to −10 km from the source as compared to C5), with the exception

Table 3
Fraction of Each FDOM Component Remaining (i.e., Intensity of C1–C5 Components Divided by Total Remaining FDOM) In-Stream 10 km Downstream of a Point Source Continuous Input, Simulated Under Transport and Reaction Conditions in August 2016, November 2016, January 2017, and May 2017

	January	May	August	November
C1[a]	0.53	0.52	0.53	0.51
C2	0.11	0.11	0.12	0.10
C3	0.13	0.13	0.13	0.14
C4	0.18	0.19	0.19	0.19
C5	0.05	0.05	0.03	0.06

[a]C1–C5 represent FDOM components. C1–C3 represent humic-like FDOM; C4 and C5 represent protein-like FDOM.

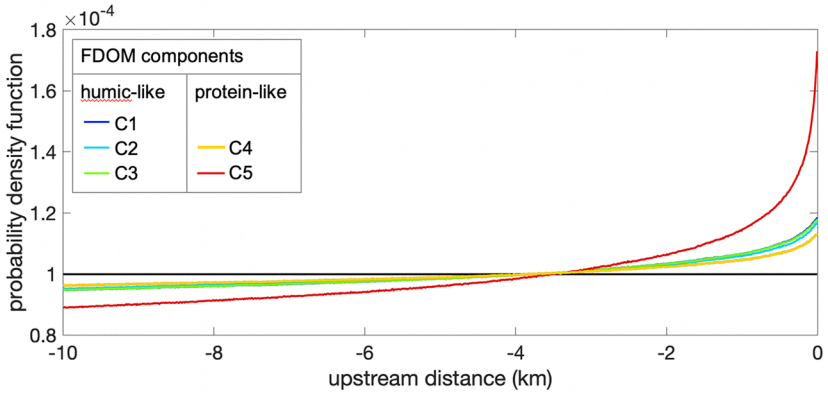

Figure 6. Upstream distribution of contributing sources for in-stream fluorescent dissolved organic matter (FDOM) components and a conservative tracer (black line), simulated under transport and reaction conditions in May 2017. Local stream water ($x = 0$) reflects the signature of dissolved organic matter (DOM) from a wide range of upstream sources (from 0 to −10 km upstream of the sampling location).

of a signature of material introduced 1–2 km upstream of the observation location (shown as around −2 to −1 km in Figure 6) that had not yet become depleted (Figure 6). The other FDOM components (C1–C3) fall in between C4 and C5 with overall more subtle changes in lability with residence time. These results clearly show that local stream water reflects the signature of DOM from a wide range of upstream sources, and the relative contribution of each upstream source depends on the labilities of each DOM component.

4. Discussion

4.1. Model Conceptualization of DOM In-Stream Dynamics

Our modeling approach allows for a new way to conceptualize reach scale DOM dynamics by allowing for lability variations in both space and time during downstream transport. Our model removes the conventional assumption of constant reaction rate and flow parameters by accounting for the vertical variations of velocity, mixing, and reaction rate across the stream-subsurface continuum, and accounts for both the range of reaction rates that comprise natural DOM and the change in reaction rate as more labile DOM is preferentially metabolized. Specifically, previous models were limited to describing uptake as discrete (up to three) DOM lability pools characterized by a constant reaction rate (Boano et al., 2014; Newbold et al., 1983; Ward & Packman, 2019). However, our model tracks the cumulative time that each discretized DOM fraction spends in the bioactive region, with the ability to account for extensive spatial and temporal resolution, and allows for dynamic changes in DOM reaction rates based on the trajectories during downstream transport. Thus, the model describes uptake of DOM spanning a continuum of labilities (Boudreau & Ruddick, 1991; Koehler et al., 2012) rather than being limited to discrete lability pools characterized by a constant reaction rate (e.g., Kaplan et al., 2008).

Overall, we show that, in the nutrient-rich headwaters of White Clay Creek, seasonal variations in bioactive residence time can be more important than seasonal variations in reaction rate constants in controlling DOM uptake (Figure 3, Table 2B). The reaction rate constant reflects the distribution of active microbial communities and how they respond to varying substrate lability and temperature over seasons, while the bioactive residence time is controlled by the distribution of active microbial communities and hydrologic conditions in each season. Many studies have found that residence time controls carbon and nutrient uptake in rivers (Battin et al., 2008; Kothawala et al., 2015; Lambert et al., 2016; Raymond et al., 2016), whereas others have found that residence time is less important than substrate availability in controlling total DOM uptake (Seybold & McGlynn, 2018). In White Clay Creek, August and November had lower discharge and shorter bioactive residence times, suggesting less hydrodynamic mixing with the bioactive streambed, while January and May had higher discharge and longer bioactive residence times (Figure 3a). Uptake velocities in January and May were higher than uptake velocities in August and November (Table 1B), despite the fact that January and August had the lowest and highest reaction rate constants, respectively (Figure 3b).

May and November had very similar reaction rate constants (Figure 3b), but the lower uptake velocity in November (Table 1B) can be explained by the lower bioactive residence time (Figure 3a). Taken together, our results suggest that stream-surface hydrodynamic mixing is an important control on bioactive residence times and influences in-stream DOM uptake.

4.2. Reach-Scale FDOM Fractionation Predicted from Model Simulations

Our combined experimental and computational approach assessed FDOM fractionation at the reach scale. Model simulations predicted reach-scale FDOM fractionation that resulted from the combined influence of hydrologic transport, residence time in bioactive regions, and decreasing biological lability with residence time (Figure 5, Table 3). These results underscore the importance of the high abundance and low lability of humic-like FDOM to stream water FDOM uptake (Figure 4, Table 2B). Indeed, a large pool of slowly degraded humic-like DOM is consistent with observations that semi-labile DOM (sensu Carlson, 2002) dominates the pool of biodegradable DOM in aquatic ecosystems and provides a degree of metabolic stability to those systems (Wetzel, 1984). Previously, operationally defined humic DOM was considered to represent the recalcitrant fraction of the DOM pool (Aiken et al., 1992). However, studies have found relatively high concentrations of biodegradable humic DOM (Volk et al., 1997).

Model simulations also showed how the interplay of hydrologic conditions and variations in biological lability of each FDOM component determine their relative abundance downstream (Figure 5, Table 3). For example, the model was able to account for the contrasting behavior of protein-like FDOM components in White Clay Creek, showing that lability variations with bioactive residence time led to reach-scale removal of tyrosine-like FDOM (C5) and reach-scale accumulation of tryptophan-like FDOM (C4) (Figure 5, Table 3). In White Clay Creek, streambed heterotrophic metabolism dominates reach-scale uptake. Given that more labile material disappears rapidly, in this stream DOM concentrations and associated uptake downstream depend more on the ability of stream microorganisms to metabolize the more recalcitrant fraction of each DOM component than on the lability of fresh DOM. The projected differences in reach-scale removal of protein-like FDOM C4 and C5 (Table 2B) highlight the need to not only measure stream water DOM fractions but also connect decreasing biological lability to bioactive residence times at the reach scale.

Our model is able to simulate the preferential accumulation of less-labile DOM. The results suggest that streams receive a wide range of DOM but transport much more lower-lability DOM (Table 2, Figure 5). This biogeochemical diversity contributes to the microbial diversity observed in headwater streams (Battin et al., 2016) by simultaneously supporting a wide range of metabolisms. In White Clay Creek the labile DOM pool represented a small fraction of the DOM in transport that is rapidly depleted by benthic and hyporheic metabolism. The headwaters we have studied are similar to larger river ecosystems in that the biodegradable DOM pool is likely a mixture of labile monomers with short uptake lengths (Newbold et al., 2006), labile fresh inputs of DOM, and a much larger pool of semi-labile DOM.

4.3. Preferential Uptake of More Biologically Labile DOM from Upstream Distributed Sources

Low concentrations of labile DOM molecules cycle rapidly within aquatic ecosystems while semi-labile and refractory DOM are present in higher concentrations but cycle slowly (Sanders et al.,1980). However, a model that can incorporate both transport and metabolism of different DOM lability pools has been lacking. Our modeling results are consistent with prior conclusions that the dominant role of bacterial metabolic scavenging of DOM and conversion to gaseous phases is a unifying property across aquatic ecosystems (Wetzel, 1984). Our model is able to demonstrate how and why DOM uptake, and hence respiratory outgassing of CO_2, may be substantially larger than can be inferred from spatial patterns of DOM concentrations within a river network. Our model showed that labile DOM can both originate and be consumed (Figure 6) over the short distances of a stream reach. Observed concentrations of labile DOM therefore reflect a local equilibration between supply and uptake, and cannot, as Wollheim et al. (2015) pointed out, reveal uptake from upstream-to-downstream concentration gradients. In contrast, removal of the semi-labile and recalcitrant fractions, by virtue of their long travel distances, is more amenable to quantification at the scale of the river network. Most of the water supply, and presumably most of the DOM supply to river networks originates in first- and second-order streams (Alexander et al., 2007; Wollheim et al., 2008).

In both the Amazon (Richey et al., 1990) and Hudson (del Giorgio & Pace, 2008) Rivers, the removal of DOM inferred from longitudinal concentration gradients was insufficient to account for observed respiration. These authors proposed an unobserved local source of rapidly cycled labile DOM to account for the discrepancy, which for White Clay Creek could include algal exudates (Kaplan and Bott, 1982; 1989) and inputs from riparian zone soils (Mei et al., 2014). Our model-data synthesis approach provides a conceptualization of DOM dynamics in streams that supports their conjectures. Furthermore, estimates of riverine outgassing at the global scale have concluded that more than half of terrestrial organic carbon inputs are lost to respiration and do not reach the sea (Cole et al., 2007; Le Quéré et al., 2015; Sawakuchi et al., 2017). In contrast, concentration-based mass-balance estimates of DOM removal within river networks report far smaller losses, and none greater than 50% (Lauerwald et al., 2012; Weyhenmeyer et al., 2012; Wollheim et al., 2015). These differences between measures of outgassing and uptake may be attributable to some extent to the degradation of locally sourced labile DOM and, if so, suggest that the degradation of locally sourced labile DOM has global implications for the carbon cycle.

4.4. Model-Data Synthesis for Improved Interpretation of DOM Dynamics in Streams

We developed a model that can account for the combined effects of in-stream and hyporheic processes on DOM dynamics in rivers, and used the model to assess the implications of bioactive subsurface processes for interpreting in-stream DOM measurements. Processes not considered in our study that may be more important in other streams, may result in higher DOM removal than we estimated. For example, photochemical processes can both mineralize DOM to CO_2 and partially degrade DOM fractions to become more or less labile to microbial respiration (Bowen et al., 2020; Cory et al., 2013; Moran et al., 2000). For larger streams, our uptake estimates are likely conservative due to the increasing role of photodegradation downstream (Cory et al., 2014). Sorption may also remove DOM from rivers in the presence of iron oxides (Aufdenkampe et al., 2001; McKnight et al., 1992). Our physically based modeling framework can be readily extended to incorporate additional mechanisms of DOM uptake, such as photochemical processes (Li et al., 2019), and future research will be needed to estimate the contribution of each mechanism to total DOM uptake in rivers. Rivers have multiscale heterogeneity in space and time (Battin et al., 2016; Boano et al., 2014; Ward & Packman, 2019). We did not consider within-reach hydrological variability on the effects of temporal changes in lability on DOM uptake and fractionation. However, preferential uptake of labile DOM is important in rivers regardless of hydrological conditions. Our model-data synthesis approach can improve interpretation of DOM dynamics in streams by demonstrating how the distribution of DOM fractions (i.e., fractionation) and spiraling metrics are dependent on in-stream location, which can reconcile apparent discrepancies between respiratory outgassing of CO_2 and longitudinal DOM concentration gradients within river networks.

Data Availability Statement

The raw data and source code used to generate the model simulations are provided online at https://doi.org/10.6084/m9.figshare.12235529.

Acknowledgments
This work was supported by National Science Foundation grants EAR-1344280 to AIP, EAR-1451372 to RMC, and DEB-1052716 and EAR-1452039 to LAK, and the European Commission supported *HiFreq: Smart high-frequency environmental sensor networks for quantifying nonlinear hydrological process dynamics across spatial scales* (project ID 734317). We thank J.D. Newbold for sharing data of solute tracer (NaCl) experiments from White Clay Creek.

References

Aiken, G. R., Mcknight, D. M., Thorn, K., & Thurman, E. (1992). Isolation of hydrophilic organic acids from water using nonionic macroporous resins. *Organic Geochemistry*, *18*(4), 567–573. https://doi.org/10.1016/0146-6380(92)90119-I

Alexander, R. B., Boyer, E. W., Smith, R. A., Schwarz, G. E., & Moore, R. B. (2007). The role of headwater streams in downstream water quality. *Journal of the American Water Resources Association*, *43*, 41–59. https://doi.org/10.1111/j.1752-1688.2007.00005.x

Aufdenkampe, A. K., Hedges, J. I., Richey, J. E., Krusche, A. V., & Llerena, C. A. (2001). Sorptive fractionation of dissolved organic nitrogen and amino acids onto fine sediments with the Amazon Basin. *Limnology and Oceanography*, *46*, 1921–1935. https://doi.org/10.4319/lo.2001.46.8.1921

Balcarczyk, K. L., Jones, J. B., Jaffé, R., & Maie, N. (2009). Stream dissolved organic matter bioavailability and composition in watersheds underlain with discontinuous permafrost. *Biogeochemistry*, *94*(3), 255–270. https://doi.org/10.1007/s10533-009-9324-x

Battin, T. J., Besemer, K., Bengtsson, M. M., Romani, A. M., & Packman, A. I. (2016). The ecology and biogeochemistry of stream biofilms. *Nature Reviews Microbiology*, *14*(4), 251–263. https://doi.org/10.1038/nrmicro.2016.15

Battin, T. J., Kaplan, L. A., Findlay, S., Hopkinson, C. S., Marti, E., Packman, A. I., et al. (2008). Biophysical controls on organic carbon fluxes in fluvial networks. *Nature Geoscience*, *1*(2), 95–100. https://doi.org/10.1038/ngeo101

Battin, T. J., Kaplan, L. A., Newbold, J. D., & Hendricks, S. P. (2003). A mixing model analysis of stream solute dynamics and the contribution of a hyporheic zone to ecosystem function. *Freshwater Biology*, *48*(6), 995–1014. https://doi.org/10.1046/j.1365-2427.2003.01062.x

Boano, F., Harvey, J. W., Marion, A., Packman, A. I., RevelliRidolfi, R. L., & Worman, A. (2014). Hyporheic flow and transport processes: Mechanisms, models, and biogeochemical implications. *Reviews of Geophysics*, *52*(4), 603–679. https://doi.org/10.1002/2012rg000417

Boudreau, B. P., Arnosti, C., Jørgensen, B. B., & Canfield, D. E. (2008). Comment on "physical model for the decay and preservation of marine organic carbon". *Science*, *319*(5870), 1616. https://doi.org/10.1126/science.1148589

Boudreau, B. P., & Ruddick, B. R. (1991). On a reactive continuum representation of organic matter diagenesis. *American Journal of Science*, *291*(5), 507–538. https://doi.org/10.2475/ajs.291.5.507

Bowen, J. C., Kaplan, L. A., & Cory, R. M. (2020). Photodegradation disproportionately impacts biodegradation of semi-labile DOM in streams. *Limnology and Oceanography*, *65*(1), 13–26. https://doi.org/10.1002/lno.11244

Brown, J. H., Gillooly, J. F., Allen, A. P., Savage, V. M., & West, G. B. (2004). Toward a metabolic theory of ecology. *Ecology*, *85*(7), 1771–1789. https://doi.org/10.1890/03-9000

Caissie, D. (2006). The thermal regime of rivers: a review. *Freshwater Biology*, *51*(8), 1389–1406. https://doi.org/10.1111/j.1365-2427.2006.01597.x

Carlson, C. A. (2002). Production and removal processes. In D. A. Hansell, & C. A. Carlson (Eds.), *Biogeochemistry of marine dissolved organic matter* (pp. 91–139). Elsevier Science, Boston: Academic Press.

Cory, R. M., Crump, B. C., Dobkowski, J. A., & Kling, G. W. (2013). Surface exposure to sunlight stimulates CO2 release from permafrost soil carbon in the Arctic. *Proceedings of the National Academy of Sciences of the United States of America*, *110*(9), 3429–3434. https://doi.org/10.1073/pnas.1214104110

Cory, R. M., & Kaplan, L. A. (2012). Biological lability of stream water fluorescent dissolved organic matter. *Limnology & Oceanography*, *57*(5), 1347–1360. https://doi.org/10.4319/lo.2012.57.5.1347

Cory, R. M., & Mcknight, D. M. (2005). Fluorescence spectroscopy reveals ubiquitous presence of oxidized and reduced quinones in dissolved organic matter. *Environmental Science & Technology*, *39*(21), 8142–8149. https://doi.org/10.1021/es0506962

Cory, R. M., Ward, C. P., Crump, B. C., & Kling, G. W. (2014). Sunlight controls water column processing of carbon in arctic freshwater. *Science*, *345*, 925–928. https://doi.org/10.1126/science.1253119

del Giorgio, P. A., & Pace, M. L. (2008). Relative independence of dissolved organic carbon transport and processing in a large temperate river: The Hudson River as both pipe and reactor. *Limnology and Oceanography*, *53*(1), 185–197. https://doi.org/10.2307/40006160

Demars, B. O., Russell Manson, J., Olafsson, J. S., Gislason, G. M., Gudmundsdottír, R., Woodward, G., et al. (2011). Temperature and the metabolic balance of streams. *Freshwater Biology*, *56*(6), 1106–1121. https://doi.org/10.1111/j.1365-2427.2010.02554.x

Fellman, J. B., Hood, E., D'amore, D. V., Edwards, R. T., & White, D. D. (2009a). Seasonal changes in the chemical quality and biodegradability of dissolved organic matter exported from soils to streams in coastal temperate rainforest watersheds. *Biogeochemistry*, *95*(2–3), 277–293. https://doi.org/10.1007/s10533-009-9336-6

Fellman, J. B., Hood, E., Edwards, R. T., & Jones, J. B. (2009b). Uptake of allochthonous dissolved organic matter from soil and salmon in coastal temperate rainforest streams. *Ecosystems*, *12*(5), 747–759. https://doi.org/10.10007/s10021-009-9254-4

Fischer, H., & Pusch, M. (2001). Comparison of bacterial production in sediments, epiphyton and the pelagic zone of a lowland river. *Freshwater Biology*, *46*(10), 1335–1348. https://doi.org/10.1046/j.1365-2427.2001.00753.x

Gillooly, J. F., Brown, J. H., West, G. B., Savage, V. M., & Charnov, E. L. (2001). Effects of size and temperature on metabolic rate. *Science*, *293*(5538), 2248–2251. https://doi.org/10.1126/science.1061967

Harun, S., Baker, A., Bradley, C., & Pinay, G. (2016). Spatial and seasonal variations in the composition of dissolved organic matter in a tropical catchment: The Lower Kinabatangan River, Sabah, Malaysia. *Environmental Sciences: Processes & Impacts*, *18*(1), 137–150. https://doi.org/10.1039/C5EM00462D

Harvey, J. W., & Gooseff, M. N. (2015). River corridor science: Hydrologic exchange and ecological consequences from bedforms to basins. *Water Resources Research*, *51*(9), 6893–6922. https://doi.org/10.1002/2015WR017617

Hood, E., Fellman, J., Spencer, R. G., Hernes, P. J., Edwards, R., D'amore, D., & Scott, D. (2009). Glaciers as a source of ancient and labile organic matter to the marine environment. *Nature*, *462*(7276), 1044. https://doi.org/10.1038/nature08580

Hullar, M. A., Kaplan, L. A., & Stahl, D. A. (2006). Recurring seasonal dynamics of microbial communities in stream habitats. *Applied & Environmental Microbiology*, *72*(1), 713–722. https://doi.org/10.1128/AEM.72.1.713-722.2006

Kaplan, L. A. (2019). Dissolved organic carbon concentrations in White Clay Creek, Pennsylvania 1977-2017 ver 1. *Environmental Data Initiative*. https://doi.org/10.6073/pasta/60deae3675ff30109bf7a35cceaf719d

Kaplan, L. A. & Bott, T. L. (1982). Diel fluctuations of DOC generated by algae in a piedmont stream. *Limnology and Oceanography*, *27*(6), 1091–1100.

Kaplan, L. A. & Bott, T. L. (1989). Diel fluctuations in bacterial activity on streambed substrata during vernal algal blooms: Effects of temperature, water chemistry, and habitat. *Limnology and Oceanography*, *34*(4), 718–733.

Kaplan, L. A., & Newbold, J. D. (1995). Measurement of stream water biodegradable dissolved organic carbon with a plug-flow bioreactor. *Water Research*, *29*(12), 2696–2706. https://doi.org/10.1016/0043-1354(95)00135-8

Kaplan, L. A., Newbold, J. D., Wiegner, T. N., & Ostrom, M. H. (2019). Stable isotope and conservative tracer data used to estimate uptake of stream water dissolved organic carbon (DOC) through a whole-stream addition of a ^{13}C-DOC tracer coupled with laboratory measurements of bioavailability of the tracer and stream water DOC using lability profiling with bioreactors ver 1. *Environmental Data Initiative*. https://doi.org/10.6073/pasta/b839940664e7c198a5472530978a1e3e

Kaplan, L. A., Wiegner, T. N., Newbold, J. D., Ostrom, P. H., & Gandhi, H. (2008). Untangling the complex issue of dissolved organic carbon uptake: a stable isotope approach. *Freshwater Biology*, *53*(5), 855–864. https://doi.org/10.1111/j.1365-2427.2007.01941.x

Koehler, B., Wachenfeldt, E., Kothawala, D., & Tranvik, L. J. (2012). Reactivity continuum of dissolved organic carbon decomposition in lake water. *Journal of Geophysical Research*, *117*, G01024. https://doi.org/10.1029/2011JG001793

Kothawala, D. N., Ji, X., Laudon, H., Ågren, A. M., Futter, M. N., Köhler, S. J., & Tranvik, L. J. (2015). The relative influence of land cover, hydrology, and in-stream processing on the composition of dissolved organic matter in boreal streams. *Journal of Geophysical Research: Biogeosciences*, *120*(8), 1491–1505. https://doi.org/10.1002/2015JG002946

Lambert, T., Teodoru, C. R., Nyoni, F. C., Bouillon, S., Darchambeau, F., Massicotte, P., & Borges, A. V. (2016). Along-stream transport and transformation of dissolved organic matter in a large tropical river. *Biogeosciences*, *13*(9), 2727–2741. https://doi.org/10.5194/bg-13-2727-2016

Lauerwald, R., Hartmann, J., Ludwig, W., & Moosdorf, N. (2012). Assessing the nonconservative fluvial fluxes of dissolved organic carbon in North America. *Journal of Geophysical Research*, *117*, 1–19. https://doi.org/10.1029/2011JG001820

Le Quéré, C., Moriarty, R., Andrew, R. M., Peters, G. P., Ciais, P., Friedlingstein, P., et al. (2015). Global carbon budget 2015. *Earth System Science Data*, *7*, 47–85. https://doi.org/10.5194/essd-7-47-2015

Li, A., Aubeneau, A. F., Bolster, D., Tank, J. L., & Packman, A. I. (2017). Covariation in patterns of turbulence-driven hyporheic flow and denitrification enhances reach-scale nitrogen removal. *Water Resources Research*, *53*(8), 6927–6944. https://doi.org/10.1002/2016WR019949

Li, A., Aubeneau, A. F., King, T., Cory, R. M., Neilson, B. T., Bolster, D., & Packman, A. I. (2019). Effects of vertical hydrodynamic mixing on photomineralization of dissolved organic carbon in arctic surface waters. *Environmental Sciences: Processes & Impacts*, *21*(4), 748–760. https://doi.org/10.1039/c8em00455b

Masese, F. O., Salcedo-Borda, J. S., Gettel, G. M., Irvine, K., & Mcclain, M. E. (2017). Influence of catchment land use and seasonality on dissolved organic matter composition and ecosystem metabolism in headwater streams of a Kenyan river. *Biogeochemistry*, *132*(1–2), 1–22. https://doi.org/10.1007/s10533-016-0269-6

McKnight, D. M., Bencala, K. E., Zellweger, G. W., Aiken, G. R., Feder, G. L., & Thorn, K. A. (1992). Sorption of dissolved organic carbon by hydrous aluminum and iron oxides occurring at the confluence of Deer Creek with the Snake River, Summit County, Colorado. *Environmental Science & Technology*, *26*(7), 1388–1396. https://doi.org/10.1021/es00031a017

Mei, Y., Hornberger, G. M., Kaplan, L. A., Newbold, J. D., & Aufdenkampe, A. K. (2014). The delivery of dissolved organic carbon from a forested hillslope to a headwater stream in southeastern Pennsylvania, USA. *Water Resources Research*, *50*, 5774–5796. https://doi.org/10.1002/2014WR015635

Minshall, G. W., Petersen, R. C., Cummins, K. W., Bott, T. L., Sedell, J. R., Cushing, C. E., & Vannote, R. L. (1983). Interbiome Comparison of Stream Ecosystem Dynamics. *Ecological Monographs*, *53*(1), 1–25.

Moran, M. A., Sheldon, W. M., & Zepp, R. G. (2000). Carbon loss and optical property changes during long-term photochemical and biological degradation of estuarine dissolved organic matter. *Limnology and Oceanography*, *45*(6), 1254–1264. https://doi.org/10.4319/lo.2000.45.6.1254

Newbold, J. D. (1992). Cycles and spirals of nutrients. In P. Calow, & G. E. Petts (Eds.), The rivers handbook: Hydrological and ecological principles (1, pp. 379–408). Oxford, UK: Blackwell Scientific Publishing.

Newbold, J. D., Bott, T. L., Kaplan, L. A., Dow, C. L., Jackson, J. K., Aufdenkampe, A. K., et al. (2006). Uptake of nutrients and organic C in streams in New York City drinking-water-supply watersheds. *Journal of the North American Benthological Society*, *25*(4), 998–1017. https://doi.org/10.1899/0887-3593(2006)025[0998:UONAOC]2.0.CO2

Newbold, J. D., Bott, T., Kaplan, L. A., Sweeney, B., & Vannote, R. (1997). Organic matter dynamics in White Clay Creek, Pennsylvania, USA. *Journal of the North American Benthological Society*, *16*(1), 46–50. https://doi.org/10.2307/1468231

Newbold, J. D., Elwood, J., O'Neill, R., & Sheldon, A. (1983). Phosphorus dynamics in a woodland stream ecosystem: a study of nutrient spiralling. *Ecology*, *64*(5), 1249–1265. https://doi.org/10.2307/1937833

Newbold, J. D., Elwood, J. W., Oneill, R. V., & Vanwinkle, W. W. (1981). Measuring nutrient spiralling in streams. *Canadian Journal of Fisheries and Aquatic Sciences*, *38*(7), 860–863. https://doi.org/10.1139/f81-114

Newbold, J. D., Mulholland, P. J., Elwood, J. W., & O'Neill, R. V. (1982). Organic Carbon Spiralling in Stream Ecosystems. *Oikos*, *38*(3), 266–272. https://doi.org/10.2307/3544663

Osburn, C. L., Handsel, L. T., Mikan, M. P., Paerl, H. W., & Montgomery, M. T. (2012). Fluorescence tracking of dissolved and particulate organic matter quality in a river-dominated estuary. *Environmental Science & Technology*, *46*(16), 8628–8636. https://doi.org/10.1021/es3007723

Parr, T. B., Cronan, C. S., Ohno, T., Findlay, S. E., Smith, S., & Simon, K. S. (2015). Urbanization changes the composition and bioavailability of dissolved organic matter in headwater streams. *Limnology and Oceanography*, *60*(3), 885–900. https://doi.org/10.1002/lno.10060

Parr, T. B., Ohno, T., Cronan, C. S., & Simon, K. S. (2014). ComPARAFAC: A library and tools for rapid and quantitative comparison of dissolved organic matter components resolved by Parallel Factor Analysis. *Limnology and Oceanography: Methods*, *12*(3), 114–125. https://doi.org/10.4319/lom.2014.12.114

Perkins, D. M., Yvon-Durocher, G., Demars, B. O., Reiss, J., Pichler, D. E., Friberg, N., et al. (2012). Consistent temperature dependence of respiration across ecosystems contrasting in thermal history. *Global Change Biology*, *18*(4), 1300–1311. https://doi.org/10.1111/j.1365-2486.2011.02597.x

Phinney, H. K., & McIntire, C. D. (1965). Effect of temperature on metabolism of periphyton communities developed in laboratory streams. *Limnology and Oceanography*, *10*(3), 341–345. https://doi.org/10.4319/lo.1965.10.3.0341

Raymond, P. A., Hartmann, J., Lauerwald, R., Sobek, S., Mcdonald, C., Hoover, M., et al. (2013). Global carbon dioxide emissions from inland waters. *Nature*, *503*(7476), 355–359. https://doi.org/10.3389/fmars.2017.0007610.1038/nature12760

Raymond, P. A., Saiers, J. E., & Sobczak, W. V. (2016). Hydrological and biogeochemical controls on watershed dissolved organic matter transport: Pulse-shunt concept. *Ecology*, *97*(1), 5–16. https://doi.org/10.1890/14-1684.1

Regnier, P., Friedlingstein, P., Ciais, P., Mackenzie, F. T., Gruber, N., Janssens, I. A., et al. (2013). Anthropogenic perturbation of the carbon fluxes from land to ocean. *Nature Geoscience*, *6*(8), 597–607. https://doi.org/10.1038/ngeo1830

Richey, J. E., Hedges, J. I., Devol, A. H., Quay, P. D., Victoria, R., & Martinelli, L. (1990). Biogeochemistry of carbon in the Amazon River. *Limnology and Oceanography*, *35*(2), 352–371. https://doi.org/10.4319/lo.1990.35.2.0352

Roulet, N., & Moore, T. R. (2006). Browning the waters. *Nature*, *444*(7117), 283–284. https://doi.org/10.1038/444283a

Runkel, R. L. (1998). One-dimensional transport with inflow and storage (OTIS): A solute transport model for streams and rivers. *US Geological Survey Water Resources Investigation Report 98-4018*. 1–73. https://doi.org/10.3133/wri984018

Saunders, G. W., Cummins, K. W., Gak, D. Z., Pieczynska, E., Straskrabova, V., & Wetzel, R. G. (1980). Organic matter and decomposers. In E. D. LeCren, & R. H. Lowe- McConnell (Eds.), *The functioning of freshwater ecosystems* (pp. 341–392). Cambridge, UK: Cambridge University Press.

Sawakuchi, H. O., Neu, V., Ward, N. D., de Lourdes, M., Barros, C., Valerio, A. M., et al. (2017). Carbon dioxide emissions along the lower Amazon River. *Frontiers in Marine Science*, *4*, 76. https://doi.org/10.3389/fmars.2017.00076

Sawyer, A., Kaplan, L. A., Lazareva, O., & Michael, H. (2014). Hydrologic dynamics and geochemical responses within a floodplain aquifer and hyporheic zone during Hurricane Sandy. *Water Resources Research*, *50*(6), 4877–4892. https://doi.org/10.1002/2013WR015101

Seybold, E., & McGlynn, B. (2018). Hydrologic and biogeochemical drivers of dissolved organic carbon and nitrate uptake in a headwater stream network. *Biogeochemistry*, *138*(1), 23–48. https://doi.org/10.1007/s10533-018-0426-1

Singh, S., Inamdar, S., Mitchell, M., & Mchale, P. P. (2014). Seasonal pattern of dissolved organic matter (DOM) in watershed sources: Influence of hydrologic flow paths and autumn leaf fall. *Biogeochemistry*, *118*(1–3), 321–337. https://doi.org/10.1007/s10533-013-9934-1

Sleighter, R. L., Cory, R. M., Kaplan, L. A., Abdulla, H. A., & Hatcher, P. G. (2014). A coupled geochemical and biogeochemical approach to characterize the bioreactivity of dissolved organic matter from a headwater stream. *Journal of Geophysical Research: Biogeosciences*, *119*(8), 1520–1537. https://doi.org/10.1002/2013JG002600

Stedmon, C. A., & Markager, S. (2005). Resolving the variability in dissolved organic matter fluorescence in a temperate estuary and its catchment using PARAFAC analysis. *Limnology and Oceanography*, *50*(2), 686–697. https://doi.org/10.4319/lo.2005.50.2.0686

Stream Solute Workshop. (1990). Concepts and methods for assessing solute dynamics in stream ecosystems. *Journal of the North American Benthological Society*, *9*, 95–119. https://doi.org/10.2307/1467445

Vähätalo, A. V., Aarnos, H., & Mäntyniemi, S. (2010). Biodegradability continuum and biodegradation kinetics of natural organic matter described by the beta distribution. *Biogeochemistry*, *100*, 227–240. https://doi.org/10.1007/s10533-010-9419-4
Volk, C. J., Volk, C. B., & Kaplan, L. A. (1997). Chemical composition of biodegradable dissolved organic matter in stream water. *Limnology and Oceanography*, *42*(1), 39–44. https://doi.org/10.4319/lo.1997.42.1.0039
Ward, A. S., & Packman, A. I. (2019). Advancing our predictive understanding of river corridor exchange. *Wiley Interdisciplinary Reviews: Water*, *6*(1), e1327. https://doi.org/10.1002/wat2.1327
Wehrli, B. (2013). Biogeochemistry: Conduits of the carbon cycle. *Nature*, *503*(7476), 346. https://doi.org/10.1038/503346a
Welter, J. R., Benstead, J. P., Cross, W. F., Hood, J. M., Huryn, A. D., Johnson, P. W., & Williamson, T. J. (2015). *Ecology*, *96*(3), 603–610.
Wetzel, R. G. (1984). Detrital dissolved and particulate organic carbon functions in aquatic ecosystems. *Bulletin of Marine Science*, *35*(3), 503–509.
Weyhenmeyer, G. A., Kortelainen, P., Sobek, S., Müller, R., & Rantakari, M. (2012). Carbon dioxide in Boreal surface waters: A comparison of lakes and streams. *Ecosystems*, *15*(8), 1295–1307. https://doi.org/10.1007/s10021-012-9585-4
Wiegner, T. N., Kaplan, L. A., Ziegler, S. E., & Findlay, R. H. (2015). Consumption of terrestrial dissolved organic carbon by stream microorganisms. *Aquatic Microbial Ecology*, *75*(3), 225–237. https://doi.org/10.3354/ame01761
Wollheim, W. M., Peterson, B. J., Thomas, S. M., Hopkinson, C. H., & Vorosmarty, C. J. (2008). Dynamics of N removal over annual time periods in a suburban river network. *Journal of Geophysical Research: Biogeosciences*, *113*, G03038. https://doi.org/10.1029/2007JG000660
Wollheim, W. M., Stewart, R. J., Aiken, G. R., Butler, K. D., Morse, N. B., & Salisbury, J. (2015). Removal of terrestrial DOC in aquatic ecosystems of a temperate river network. *Geophysical Research Letters*, *42*(16), 6671–6679. https://doi.org/10.1002/2015GL064647

References From the Supporting Information

Bear, J. (1972). *Dynamics of fluids in porous media*. New York, NY: Dover.
Beavers, G. S., & Joseph, D. D. (1967). Boundary conditions at a naturally permeable wall. *Journal of Fluid Mechanics*, *30*, 197–207 https://doi.org/10.1017/s0022112067001375
Chakraborty, P., Meerschaert, M. M., & Lim, C. Y. (2009). Parameter estimation for fractional transport: A particle-tracking approach. *Water Resources Research*, *45*(10), W10415. https://doi.org/10.1029/2008WR007577
Delay, F., Ackerer, P., & Danquigny, C. (2005). Simulating solute transport in porous or fractured formations using random walk particle tracking: A review. *Vadose Zone Journal*, *4*(2), 360–379. https://doi.org/10.2136/vzj2004.0125
Elliott, A. H., & Brooks, N. H. (1997a). Transfer of nonsorbing solutes to a streambed with bed forms: Theory. *Water Resources Research*, *33*(1), 123–136. https://doi.org/10.1029/96wr02784
Elliott, A. H., & Brooks, N. H. (1997b). Transfer of nonsorbing solutes to a streambed with bed forms: Laboratory experiments. *Water Resources Research*, *33*(1), 137–151. https://doi.org/10.1029/96WR02783
Fischer, H. B. (1966). *Longitudinal dispersion in laboratory and natural streams* (W. M. Keck Laboratory of Hydraulics and Water Resources Report 12). Pasadena, CA: California Institute of Technology. https://doi.org/10.7907/Z9F769HC
Fischer, H. B. (1967). The mechanics of dispersion in natural streams. *Journal of the Hydraulics Division*, *93*(6), 187–216.
Fischer, H. B., List, J. E., Koh, C. R., Imberger, J., & Brooks, N. H. (1979). *Mixing in inland and coastal waters*, San Diego: Academic.
Kinzelbach, W. (1988). The random walk method in pollutant transport simulation. In Custodio, E., Gurgui, A., & Ferreira, J. P. L. (Eds.), Groundwater flow and quality modelling (Vol. 224, pp. 227–245). Dordrecht: Springer. https://doi.org/10.1007/978-94-009-2889-3_15
Manes, C., Poggi, D., & Ridolfi, L. (2011). Turbulent boundary layers over permeable walls: Scaling and near-wall structure. *Journal of Fluid Mechanics*, *687*, 141–170. https://doi.org/10.1017/jfm.2011.329
Mendoza, C., & Zhou, D. H. (1992). Effects of porous bed on turbulent stream flow above bed. *Journal of Hydraulic Engineering: ASCE*, *118*(9), 1222–1240. https://doi.org/10.1061/(asce)0733-9429
Nagaoka, H., & Ohgaki, S. (1990). Mass transfer mechanism in a porous riverbed. *Water Research*, *24*(4), 417–425. https://doi.org/10.1016/0043-1354(90)90223-s
Prickett, T. A., Naymik, T. G., Lonnquist, C. G., & Survey, I. S. W. (1981). A "random-walk" solute transport model for selected groundwater quality evaluations. *Illinois State Water Survey Bulletin*, *65*.1–103.
Wetzel, R. G., Hatcher, P. G., & Bianchi, T. S. (1995). Natural photolysis by ultraviolet irradiance of recalcitrant dissolved organic matter to simple substrates for rapid bacterial metabolism. *Limnology and Oceanography*, *40*(8), 1369–1380.
Zhou, D. H., & Mendoza, C. (1993). Flow through porous bed of turbulent stream. *Journal of Engineering Mechanics: ASCE*, *119*(2), 365–383. https://doi.org/10.1061/(asce)0733-9399